

Stability of elastoviscoplastic plane Couette flow

Ramkarn Patne^{1†}

¹Department of Chemical Engineering, Indian Institute of Technology Hyderabad, Kandi, Sangareddy, Telangana 502285, India

(Received xx; revised xx; accepted xx)

Several studies have investigated the turbulent flow of elastoviscoplastic (EVP) fluids, which exhibit yield stress in addition to viscoelasticity. The instabilities that could be responsible for the transition to turbulence in the EVP fluid flows remain unknown. Thus, the present explores the linear stability of EVP plane Couette flow (PCF) by employing Saramito model. The eigenvalue problem is solved by using pseudo-spectral method. In the limit of vanishing yield stress, EVP fluid behaves as Upper Convected Maxwell (UCM) fluid. The creeping flow of UCM fluid exhibits two stable Gorodotsov & Leonov (GL) modes, thus a stable flow. As the Bingham number (i.e., yield stress) increases, the GL modes become unstable, implying an unstable flow. Additionally, there are new unstable modes with phase speed equalling the average velocity of the fluid. The analysis reveals an extra tangential stress term, arising due to yield stress, is responsible for the predicted instabilities. Also, the Saramito model exhibits weak Hadamard instability, i.e., unstable perturbations of arbitrarily small wavelengths. The present study demonstrates the removal of the Hadamard instability by adding a stress diffusion term in the Saramito constitutive equation. To conclude, the PCF of an EVP fluid is linearly unstable.

Key words:

1. Introduction

Elastoviscoplastic (EVP) fluids or viscoelastic fluids possessing yield stress are common in nature (e.g., mud and lava) (Abdelgawad *et al.* 2023), industrial applications (e.g., Carbopol gels and concrete) (Barry & Meyer 1979; Abdelgawad *et al.* 2023) and biosystems (e.g., blood and airway mucus) (Apostolidis & Beris 2014; Erken *et al.* 2023; Shemilt *et al.* 2022, 2023). Recently, Rosti *et al.* (2018); Izbassarov *et al.* (2021); Abdelgawad *et al.* (2023) have investigated the turbulent flow of EVP flows. However, the instabilities which could be responsible for the turbulent flow remain a mystery. The present study is an effort to address this missing gap. Below, we review the relevant literature.

1.1. Bingham fluid flows

An EVP fluid exhibits yield stress; thus, below, we review the relevant literature. Bingham (1922) proposed a one-dimensional constitutive model to describe the flow of yield stress fluids. His model assumed that the material behaves as a rigid body before yielding and as a Newtonian fluid after yielding. The stability of plane Poiseuille flow of Bingham fluid was first investigated by Frigaard *et al.* (1994). Their analysis

† Email address for correspondence: ramkarn@che.iith.ac.in

predicted that the critical Reynolds number for the onset of unstable flow increases with increasing Bingham number. Later, Nouar *et al.* (2007b) studied the same problem, but he employed the Chebyshev collocation method to solve the eigenvalue problem. Their analysis predicted that the plane Poiseuille flow of a Bingham fluid is linearly stable. The disagreement between the predictions of Frigaard *et al.* (1994) and Nouar *et al.* (2007b) was due to the erroneous numerical method employed by the former to compute the eigenvalues. Note that the plane Poiseuille flow of a Newtonian fluid exhibits Tollmien-Schlichting instability with critical Reynolds number 5772. This clearly demonstrates the role of yield stress in suppressing instabilities.

Peng & Zhu (2004) investigated the linear stability of Bingham fluids in spiral Couette flow and concluded the stabilizing effect of yield stress on flow. Landry *et al.* (2005) investigated the stability of Taylor–Couette flows of a Bingham fluid by considering three cases, viz., fully unyielded, partially yielded and fully yielded. Only solid body rotation is possible in the fully unyielded case since the Bingham fluid treats unyielded fluid as a rigid body. This will arise if the imparted stresses are lower than the yield stress of the fluid through the annular gap. If the imparted stress is sufficient to yield part of the fluid region, then the partially yielded case arises. If the imparted stress exceeds the yield stress of fluid throughout the fluid domain, then the fluid is fully yielded. A similar case of fully yielded Bingham fluid has been previously considered by Sahu *et al.* (2007) while analysing the two-layer flow of Newtonian and Bingham fluids. In the present study, following Landry *et al.* (2005); Sahu *et al.* (2007) a fully yielded flow is considered as described in Sec. 2. An excellent review of studies investigating the stability of Bingham fluid flows is given by Balmforth *et al.* (2014).

1.2. Viscoelastic fluid flows

In addition to yield stress, an EVP fluid also exhibits elasticity. Thus, next, we review the relevant literature dealing with the stability of viscoelastic fluid flows.

Gorodtsov & Leonov (1967) analysed the linear stability of Upper Convected Maxwell (UCM) plane Couette flow (PCF) in the creeping-flow, i.e., in inertialess limit. They predicted two stable discrete modes (henceforth referred to as *GL* modes). Wilson *et al.* (1999) extended analysis of Gorodtsov & Leonov (1967) to include solvent and predicted a stable flow for $W \sim O(1)$. Renardy & Renardy (1986) extended previous analyses to a finite Reynolds number and predicted a linearly stable flow for arbitrary *Re*. Nouar *et al.* (2007a) analysed the stability of PCF of an inelastic shear-thinning (power-law) fluid and predicted a linearly stable flow at low *Re*. Grillet *et al.* (2002) analysed the PCF of Giesekus (1982) and Thien & Tanner (1977) (PTT) models in the creeping-flow limit. Their analysis predicted that the PCF of a Giesekus fluid is linearly stable. In contradistinction, the PCF of the PTT fluid was found to be linearly unstable for a highly shear-thinning viscoelastic fluid at a high Weissenberg number. Arora *et al.* (2004) predicted a linearly stable PCF of pom-pom fluid in the creeping-flow limit.

The analysis by Morozov & van Saarloos (2005) predicted a purely elastic subcritical instability in PCF of UCM fluid. Hoda *et al.* (2008, 2009) explored the transient growth of perturbations for inertialess viscoelastic PCF and suggested a nonmodal route to transition. Chokshi & Kumaran (2009); Cromer *et al.* (2013, 2014); Beneitez *et al.* (2023); Couchman *et al.* (2024) considered coupling between the polymer stress and concentration and predicted a linearly unstable PCF. This coupling modifies the governing equations by the addition of the polymer concentration convection-diffusion equation. Such a coupling will not be considered in the present study. Recently, Garg *et al.* (2018); Chaudhary *et al.* (2019, 2021); Khalid *et al.* (2021); Dong & Zhang (2022) have extensively analysed the impact of fluid elasticity on pressure-driven flows. A detailed

literature review of studies concerned with the effect of elasticity on flow dynamics can be found in Datta (2022). Samanta *et al.* (2013); Choueiri *et al.* (2018); Chandra *et al.* (2018) have experimentally demonstrated the impact of fluid elasticity on flow dynamics.

The combined effect of elasticity and power-law type shear-thinning in the absence of yield stress was analysed by Wilson & Rallison (1999); Wilson & Loridan (2015); Castillo & Wilson (2017). Wilson & Rallison (1999); Wilson & Loridan (2015); Castillo & Wilson (2017) analysed the linear stability of pressure-driven channel flow of White & Metzner (1963) fluid using the power-law model for the viscosity and relaxation time and a constant relaxation modulus. Their analysis predicted an unstable flow provided the power-law index n is less than 0.3 in the creeping-flow limit. The predicted instability was experimentally observed by Bodiguel *et al.* (2015). The experiments by Poole (2016); Picaut *et al.* (2017); Wen *et al.* (2017); Chandra *et al.* (2019) further demonstrated the existence of shear-thinning elastic instabilities for the flows of concentrated polymer solutions for low Reynolds number.

1.3. Elastoviscoplastic (EVP) fluid flows

The fluids encountered in natural settings and industrial processes could possess yield stress and behave as viscoelastic fluid upon yielding. The above-discussed studies consider these properties separately. Moyers-Gonzalez *et al.* (2011) analysed the linear stability of Plane Poiseuille flow of an EVP fluid using a revised version of the Putz & Burghelea (2009) model. Their analysis concluded that stability results are in close conformity with those of a pseudo-plastic fluid. To describe the flows of EVP fluids, Saramito (2007) developed a constitutive equation which satisfies the second law of thermodynamics. As per the model, the unyielded state of the material is a neo-Hookean solid, and the yielded state is a viscoelastic Oldroyd-B fluid. The Saramito (2007) model predicts a smooth transition between the solid and liquid state due to yielding transition being based on the von Mises criterion. The predictions of the Saramito (2007) model are in excellent agreement with the experimental observations (Fraggedakis *et al.* 2016). The Saramito (2007) model has been extensively utilised to analyse turbulent flow in EVP fluid flows by Rosti *et al.* (2018); Izbassarov *et al.* (2021); Abdelgawad *et al.* (2023). To the best of the author's knowledge, the linear stability of EVP fluid modelled by Saramito (2007) constitutive equation has not been analysed. Owing to this, in the present study, we will utilise the Saramito (2007) model to analyse the linear stability of EVP plane Couette flow (PCF).

The rest of the paper is organised as follows. The base state quantities and linearised perturbation equations are derived in Sec. 2. The numerical methodology utilised to solve the eigenvalue problem and its validation is discussed in Sec. 3. Section 4 discusses the stability results, the physical mechanism responsible for the existence of the predicted instabilities, and the removal of the Hadamard instability. The salient results and implications of the present work are summarised in Sec. 5.

2. Problem formulation

Consider an incompressible EVP fluid of yield stress τ_0^* , viscosity η^* and relaxation modulus G^* flowing through the gap of width R^* between two plates. The lower plate (at $y^* = 0$) is stationary while the upper plate (at $y^* = R^*$) is moving at a steady and constant speed V^* in the positive x direction. Here, superscript $*$ signifies a dimensional

quantity. The dimensional Saramito (2007) model is

$$\frac{1}{G^*} \left[\frac{\partial \boldsymbol{\tau}^*}{\partial t^*} + (\mathbf{v}^* \cdot \nabla^*) \boldsymbol{\tau}^* - (\nabla^* \mathbf{v}^*)^T \cdot \boldsymbol{\tau}^* - \boldsymbol{\tau}^* \cdot (\nabla^* \mathbf{v}^*) \right] + \max \left(0, \left[\frac{|\boldsymbol{\tau}_d^*| - \tau_0^*}{\eta^* |\boldsymbol{\tau}_d^*|} \right] \right) \boldsymbol{\tau}^* = \dot{\boldsymbol{\gamma}}^*, \quad (2.1)$$

where $\boldsymbol{\tau}^*$ is the stress field. The deviatoric stress tensor $\boldsymbol{\tau}_d^* = \boldsymbol{\tau}^* - 1/N \text{tr}(\boldsymbol{\tau}^*)$ where N is the number of dimensions and $|\boldsymbol{\tau}_d^*| = \sqrt{1/2 \boldsymbol{\tau}_d^* : \boldsymbol{\tau}_d^*}$ (Saramito 2007; Fraggedakis *et al.* 2016). The strain rate tensor is $\dot{\boldsymbol{\gamma}}^* = (\nabla^* \mathbf{v}^*) + (\nabla^* \mathbf{v}^*)^T$. As per the von Mises criterion followed by Saramito (2007) model, when $\boldsymbol{\tau}_d^*$ exceeds the yield stress of the fluid, the material starts flowing obeying the Maxwell constitutive equation.

We scale the lengths and velocities by R^* , V^* while the stresses and pressure are scaled by $\eta^* V^*/R^*$. Let $\mathbf{v} = (v_x, v_y, v_z)$ be the velocity field, and p is the pressure field in the fluid. For the sake of simplicity, we assume the absence of solvent and creeping-flow limit. Thus, the dimensionless governing equations are

$$\nabla \cdot \mathbf{v} = 0, \quad (2.2a)$$

$$-\nabla p + \nabla \cdot \boldsymbol{\tau} = 0, \quad (2.2b)$$

$$W \left[\frac{\partial \boldsymbol{\tau}}{\partial t} + (\mathbf{v} \cdot \nabla) \boldsymbol{\tau} - (\nabla \mathbf{v})^T \cdot \boldsymbol{\tau} - \boldsymbol{\tau} \cdot (\nabla \mathbf{v}) \right] + \max \left(0, \left[\frac{|\boldsymbol{\tau}_d| - B}{|\boldsymbol{\tau}_d|} \right] \right) \boldsymbol{\tau} = \dot{\boldsymbol{\gamma}}, \quad (2.2c)$$

where, $B = \tau_0^* R^*/(\eta^* V^*)$ is the Bingham number, $W = \eta^* V^*/(G^* R^*)$ is the Weissenberg number and ∇ is the gradient operator.

The base state quantities for the flow under consideration have been obtained by Fraggedakis *et al.* (2016) using the following procedure. For PCF, owing to the constant shear stress throughout the fluid domain, either the fluid can be fully unyielded or yielded depending on the value of $|\boldsymbol{\tau}_d^*|$ and τ_0^* . In the present study, we consider fully yielded fluid for which $|\boldsymbol{\tau}_d^*| > \tau_0^*$. Note that previously, Landry *et al.* (2005) considered a similar fully yielded flow for Taylor-Couette flow while Sahu *et al.* (2007) considered a fully yielded flow for a two-layer flow of Bingham and Newtonian fluids. For a fully developed, two-dimensional steady flow, the base state quantities are

$$\bar{v}_x = y; \quad \bar{\tau}_{xx} = 2W \bar{\tau}_{xy}^2; \quad \bar{\tau}_{yy} = 0, \quad (2.3a)$$

$$\mathcal{F} \bar{\tau}_{xy} = 1; \quad \mathcal{F} = \frac{|\bar{\boldsymbol{\tau}}_d| - B}{|\bar{\boldsymbol{\tau}}_d|}; \quad |\bar{\boldsymbol{\tau}}_d| = \sqrt{\frac{\bar{\tau}_{xx}^2}{4} + \bar{\tau}_{xy}^2}. \quad (2.3b)$$

To obtain base state stress tensor components, the above equation must be solved for $\bar{\tau}_{xy}$ for specified values of W, B and n using a root-finding algorithm. In the present study, we employ *fsolve* MATLAB function to solve the above transcendental set of equations for $\bar{\tau}_{xy}$. The obtained root is further confirmed by *FindRoot* and *NSolve* functions in MATHEMATICA. For $B = 0$, the above equations yield $\bar{\tau}_{xy} = 1$ and $\bar{\tau}_{xx} = 2W$ applicable to PCF of Upper Convected Maxwell fluid. Fraggedakis *et al.* (2016) utilised Newton's method to solve the above transcendental equations.

For the sake of simplicity, we assume two-dimensional perturbations, $f'(\mathbf{x}, t) = \tilde{f}(y) e^{i k (x - ct)}$ imposed on the above base-state where $f'(\mathbf{x}, t)$ is any perturbation to dynamical variable and $\tilde{f}(y)$ is the corresponding eigenfunction. Here, k and $c = c_r + ic_i$ are the wavenumber and complex wavespeed, respectively. The flow is unstable if at least one eigenvalue satisfies the condition $c_i > 0$.

The governing equations (2.2) are linearised around the base state (2.3). In the resulting

linearised equations, the normal modes are substituted to obtain

$$ik\tilde{v}_x + D\tilde{v}_y = 0, \quad (2.4a)$$

$$-ik\tilde{p} + ik\tilde{\tau}_{xx} + D\tilde{\tau}_{xy} = 0, \quad (2.4b)$$

$$-D\tilde{p} + ik\tilde{\tau}_{xy} + D\tilde{\tau}_{yy} = 0, \quad (2.4c)$$

where $D = d/dy$. The constitutive equation (2.2c) gives

$$W[ik(\tilde{v}_x - c)\tilde{\tau}_{xx} + \tilde{v}_y D\tilde{\tau}_{xx} - 2ik\tilde{\tau}_{xx}\tilde{v}_x - 2D\tilde{v}_x\tilde{\tau}_{xy} - 2\tilde{\tau}_{xy}D\tilde{v}_x] \\ + \mathcal{F}[1 + (t_4 - t_2)\tilde{\tau}_{xx}]\tilde{\tau}_{xx} + \mathcal{F}(t_3 - t_1)\tilde{\tau}_{xx}\tilde{\tau}_{xy} - \mathcal{F}(t_4 - t_2)\tilde{\tau}_{xx}\tilde{\tau}_{yy} = 2ik\tilde{v}_x, \quad (2.4d)$$

$$W[ik(\tilde{v}_x - c)\tilde{\tau}_{xy} + \tilde{v}_y D\tilde{\tau}_{xy} - ik\tilde{\tau}_{xy}\tilde{v}_x - D\tilde{v}_x\tilde{\tau}_{yy} - ik\tilde{\tau}_{xx}\tilde{v}_y - \tilde{\tau}_{xy}D\tilde{v}_y] \\ + \mathcal{F}[1 + (t_3 - t_1)\tilde{\tau}_{xy}]\tilde{\tau}_{xy} + \mathcal{F}\tilde{\tau}_{xy}(t_4 - t_2)(\tilde{\tau}_{xx} - \tilde{\tau}_{yy}) = (ik\tilde{v}_y + D\tilde{v}_x), \quad (2.4e)$$

$$W[ik(\tilde{v}_x - c)\tilde{\tau}_{yy} - 2ik\tilde{\tau}_{xy}\tilde{v}_y] + \mathcal{F}\tilde{\tau}_{yy} = 2D\tilde{v}_y, \quad (2.4f)$$

where

$$t_1 = \frac{\tilde{\tau}_{xy}}{|\tilde{\tau}_d|^2}; \quad t_2 = \frac{\tilde{\tau}_{xx}}{4|\tilde{\tau}_d|^2}; \quad t_3 = \frac{\tilde{\tau}_{xy}}{|\tilde{\tau}_d|(|\tilde{\tau}_d| - B)}; \quad t_4 = \frac{\tilde{\tau}_{xx}}{4|\tilde{\tau}_d|(|\tilde{\tau}_d| - B)}, \quad (2.4g)$$

are the parameters arising during linearisation. The above equations are subjected to the following boundary conditions. For $B = 0$, from the above expressions, $t_1 = t_3$ and $t_2 = t_4$ which will remove the additional terms in the linearised constitutive equations (2.4d)-(2.4f) and reduce $\mathcal{F} = 1$. Thus, the additional terms in equations (2.4d)-(2.4f) compared to a UCM fluid are clearly due to nonzero yield stress.

At both plates ($y = 0, 1$), we impose no-slip and impermeability conditions, implying

$$\tilde{v}_x = 0; \quad \tilde{v}_y = 0. \quad (2.5a)$$

3. Numerical methodology

In the pseudo-spectral method, the eigenfunctions for each dynamic field are expanded into a series of the Chebyshev polynomials as

$$\tilde{f}(y) = \sum_{n=0}^{n=N} b_n \mathcal{T}_n(y), \quad (3.1)$$

where $\mathcal{T}_n(y)$ are Chebyshev polynomials of degree n , b_n are series coefficients, and N is the highest degree of the polynomial in the series expansion or, equivalently, the number of collocation points. Upon substitution of the above series expansion in (2.4) and (2.5) results in an eigenvalue problem of the form

$$\mathbf{A}\mathbf{e} + c\mathbf{B}\mathbf{e} = 0, \quad (3.2)$$

where \mathbf{A} and \mathbf{B} are the discretised matrices and \mathbf{e} is the vector of b_n .

The details of the discretisation procedure and construction of the matrices can be found in Trefethen (2000) and Schmid & Henningson (2001). We use the *eig* MATLAB routine to solve the eigenvalue problem (3.2). To filter out the spurious modes from the genuine, numerically computed spectrum of the problem, the latter is determined for N and $N + 2$ collocation points, and the eigenvalues are compared with a priori specified tolerance 10^{-5} .

As mentioned in Sec. 1, the PCF of a UCM fluid exhibits two discrete, stable GL modes in the creeping-flow limit. Following Gorodtsov & Leonov (1967), these modes can be

analytically calculated as follows. To remove the yield stress effect, substitute $B = 0$ in equations (2.4). After some algebraic manipulation the resulting equations reduce to (Gorodtsov & Leonov 1967)

$$(y_n^2 D^2 - 2y_n D - k^2 y_n^2 + 2)(D^2 + 2ikD - 2k^2 W^2 - k^2) \tilde{v}_y = 0, \quad (3.3)$$

where $y_n = y - c - i/(kW)$. The solution of the above differential equation is

$$\begin{aligned} \tilde{v}_y = & \frac{a_1(c - y_n)}{2k^2 W(i + W)} \exp(kc + i/W - ky_n) + \frac{a_2(c - y_n)}{4k^3 W(-i + W)} \exp(-kc - i/W + ky_n) \\ & + a_3 \exp \left[\frac{-\left(ikW + \sqrt{k^2(1 + W^2)}\right)(-i - kcW + kW y_n)}{kW} \right] \\ & + a_4 \exp \left[\frac{\left(-ikW + \sqrt{k^2(1 + W^2)}\right)(-i - kcW + kW y_n)}{kW} \right]. \end{aligned} \quad (3.4)$$

where a_1, a_2, a_3 and a_4 are integration constants. Substituting the above solution in the boundary conditions (2.5) leads to a dispersion relation, which can then be solved for the eigenvalue c for specified values of k and W by employing a transcendental root finding scheme in MATLAB.

From the above discussion, for $B = 0$, the present numerical methodology should predict two stable converged eigenvalues as the number of collocation points is varied. This procedure has been implemented in figure 1 for a set of parameters. Despite a change in the number of collocation points, the discrete GL modes exhibit negligible change. Furthermore, by utilizing the analytical expressions (3.4), the obtained eigenvalues are in excellent agreement with the numerically predicted eigenvalues, thereby validating the present numerical methodology. On the other hand, the continuous spectrum varies with the change in collocation points. Note that as the Weissenberg number W , Bingham number B and wavenumber k increase, the number of collocation points required to capture the most unstable eigenvalue also increases.

4. Results and Discussion

As discussed in Sec. 3, a PCF of UCM fluid exhibits two stable GL modes. Thus, first, we analyse the effect of yield stress on the GL modes by varying the Bingham number (B) in figure 2. From figure 2a, for $W = 1$ and $B = 12$, the GL modes exhibit $c_i > 0$, implying unstable GL modes. Further, to confirm the genuine nature of the modes, the spectrum is obtained for three values of the number of collocation points. The convergence of the unstable mode implies the existence of genuinely unstable modes. Further, similar to the stable GL modes, the unstable GL modes also exhibit the same c_i value, albeit with $c_i > 0$.

How are we sure that these unstable modes are GL modes? To verify this, the Bingham number is increased from $B = 0$ to $B = 12$ in steps of 0.1 as shown in figure 2b. As B increases beyond 11, the GL modes become unstable. Note that the same curve is applicable for both GL modes due to the equal c_i value. This clearly establishes that owing to the yield stress, the GL modes become unstable, leading to an unstable flow.

From figure 3, as the Bingham number is increased, the c_r values of both GL modes approach 0.5 for $k < 1$. Upon further increase in B , the GL modes merge to give rise to two modes with $c_r = 0.5$ and different c_i values. The average velocity of the PCF under consideration is 0.5. The fluid at $y = 0.5$ travels at a speed = 0.5. Since these new modes

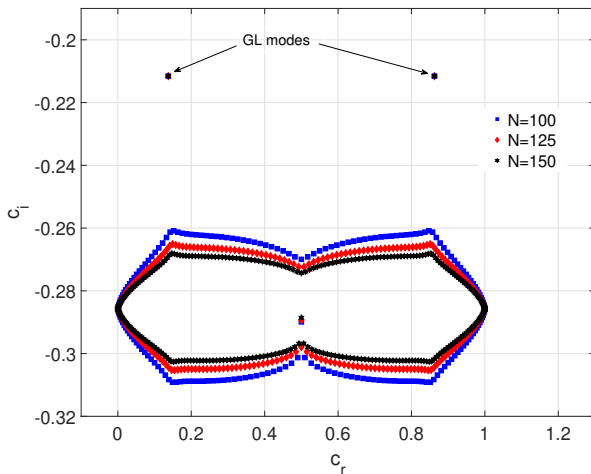
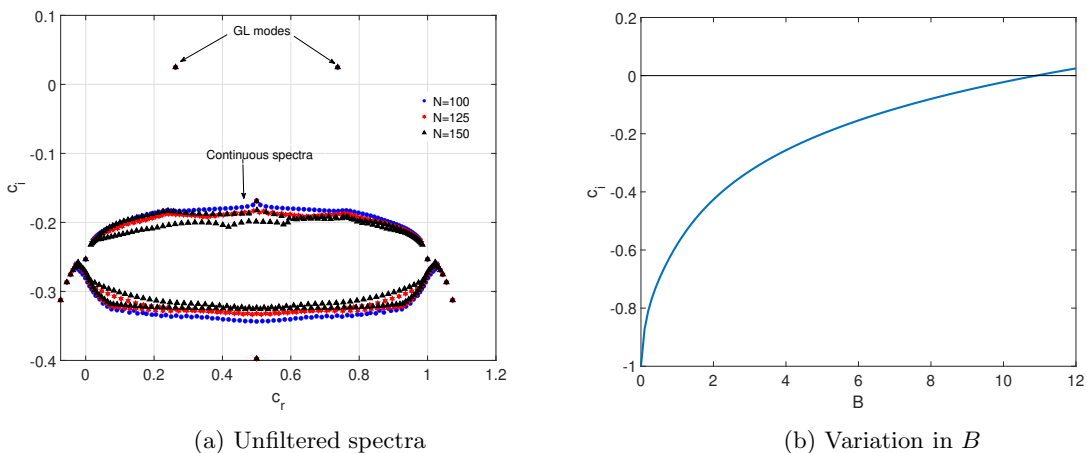


Figure 1: The variation of the discrete GL modes and continuous spectrum due to variation in the number of collocation points at $W = 5$, $B = 0$ and $k = 0.7$. The GL modes exhibit negligible variation despite an increase in the number of collocation points.



(a) Unfiltered spectra

(b) Variation in B

Figure 2: Eigenspectra for $W = 1$ and $k = 1$. Panel (a) shows the converged unstable GL modes for $B = 12$. Panel (b) demonstrates GL mode destabilisation due to the increasing yield stress effect, i.e., Bingham number B . Note that $c_i > 0$ implies an unstable mode.

travel at an average speed of the fluid, these modes will be referred to as ‘centre modes’ to differentiate them from the GL modes.

The new centre modes also become unstable for the same parameters as the GL modes. This aspect is demonstrated in figure 4. To further ascertain the genuine nature of the centre modes, spectra are obtained for three values of the number of collocation points as shown in figure 4a. The convergence of the unstable centre mode ascertains the genuine nature. The destabilisation of the centre modes due to an increasing Bingham number is illustrated in figure 4b. The centre modes become unstable for $B > 10.5$, similar to the GL modes. To conclude, along with the GL modes, the yield stress of the fluid also destabilises a new class of centre modes.

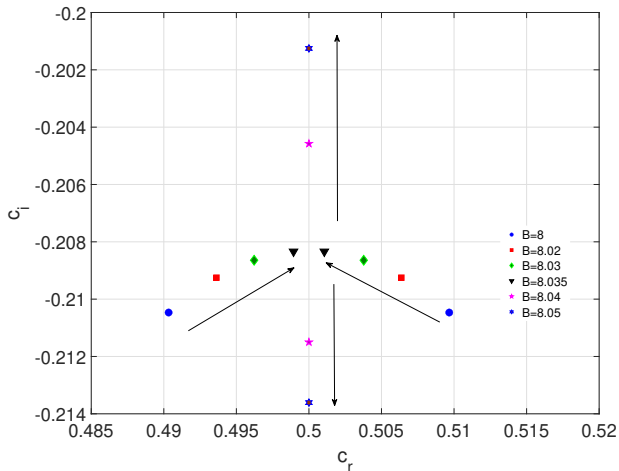
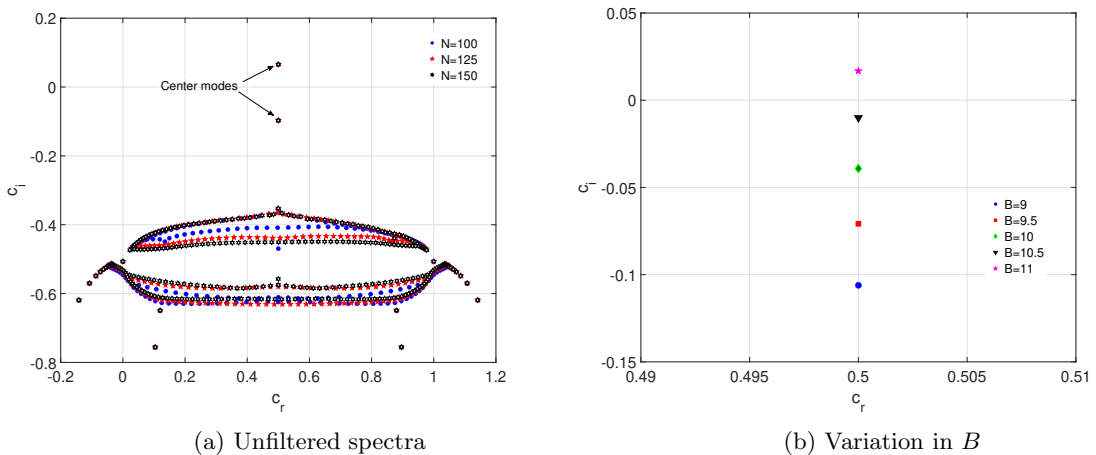


Figure 3: The manifestation of centre modes due to an increase in the Bingham number for $W = 1$ and $k = 0.5$. The GL modes merge and give rise to two modes with $c_r = 0.5$, henceforth referred to as centre modes.



(a) Unfiltered spectra

(b) Variation in B

Figure 4: Eigenspectra for $W = 1$ and $k = 0.5$ for center modes. Panel (a) shows the converged unstable centre mode for $B = 12$. Panel (b) demonstrates centre mode destabilisation due to the increasing Bingham number B . Note that $c_i > 0$ implies an unstable mode.

The preceding discussion considers the movement of eigenvalues for individual wavenumber as the Bingham number is varied. To obtain a holistic picture for a range of wavenumbers, dispersion plots are shown in figure 5a. For low Bingham numbers, the flow is stable since $c_i < 0$ for the whole range of wavenumbers. As the Bingham number is increased, the dispersion curve crosses the $c_i = 0$ threshold for a range of wavenumbers, thereby indicating an unstable flow. Additionally, the dispersion curves exhibit two distinct maxima due to the unstable centre and GL modes, i.e., two different types of modes of instability.

To determine the range of unstable wavenumber due to both types of modes, the

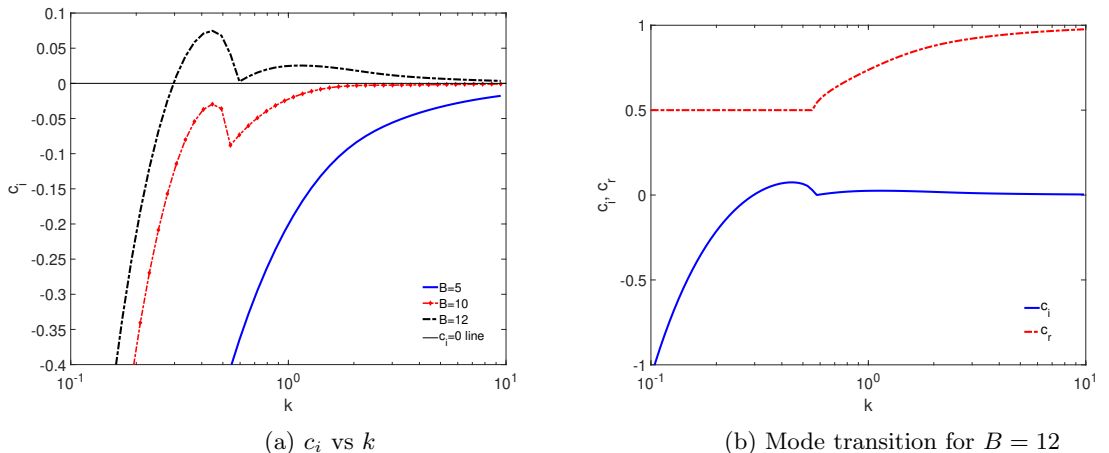


Figure 5: The dispersion curves for $W = 1$. Panel (a) shows the destabilisation of a range of wavenumber as B increases. Panel (b) shows the switching of the most unstable mode from centre mode to GL mode characterised by a change in $c_r = 0.5$ to $c_r > 0.5$. There is one more GL mode (not shown here) with the same c_i but $c_r < 0.5$.

variation of both c_r and c_i is plotted in figure 5b. For $k < 0.6$, the mode with $c_r = 0.5$ exhibits $c_i > 0$, indicating the presence of centre mode. In contrast, for $k > 0.6$, the mode with $c_r > 0.5$ exhibits $c_i > 0$ implying presence of unstable GL mode with $c_r > 0.5$. Note that for $k > 0.6$, there is one more GL mode that exists with the same c_i but with $c_r < 0.5$.

An interesting observation from figure 5a is the existence of instability at arbitrarily high wavenumber with a decreasing c_i , a phenomenon referred to as the ‘weak Hadamard instability’ (Joseph & Saut 1986). The ‘Hadamard instability’ is generally a consequence of neglecting a dissipative or stabilizing effect such as solvent viscosity (Joseph & Saut 1986), interfacial tension (Patne & Shankar 2018), or stress diffusivity (Patne *et al.* 2024). In the present case, the Hadamard instability can be removed by including stress diffusivity as discussed in Sec. 4.2.

4.1. Physical mechanism

As mentioned several times in the preceding discussion, the GL modes are linearly stable for a UCM fluid. However, as demonstrated in figures 2b and 4b, an increasing Bingham number leads to the destabilisation of the GL modes. Also, it gives rise to a new type of centre mode instability. For the existence of an instability, a term containing base state and perturbation quantities is typically responsible. Clearly, the terms which existed for a UCM fluid could not be responsible for the predicted instability owing to the stable GL modes. However, new terms arising as a result of the yield stress in the Saramito (2007) model could be responsible for this.

To check the term responsible for the predicted instability, the individual term is removed, and its effect on the eigenvalue is observed. This procedure is repeated for all the new terms arising due to the yield stress in equations (2.4d)-(2.4f). The exercise concludes that the term $\mathcal{F}(t_3 - t_1)\bar{\tau}_{xy}\tilde{\tau}_{xx}$ in equation (2.4e) is responsible for the destabilisation. Upon using the base state equations (2.3), the term further simplifies to $(t_3 - t_1)\tilde{\tau}_{xx}$. Thus, this term gives rise to an *extra tangential stress* which leads to the destabilisation. The role of this term in destabilisation is illustrated in table 1. To conclude, the fluid

Parameters	With extra tangential stress term	Without extra tangential stress term
$W = 1, B = 12, k = 1$	$0.737074 + 0.02482258i$	$0.916623 - 0.140563i$
$W = 1, B = 12, k = 0.5$	$0.500000 + 0.0655863i$	$0.833158 - 0.290123i$
$W = 2, B = 20, k = 2$	$0.929200 + 0.01916997i$	$0.976722 - 0.0377764i$
$W = 2, B = 20, k = 0.3$	$0.500000 + 0.0347959i$	$0.847715 - 0.268481i$

Table 1: A comparison of the most unstable (or least stable) eigenvalue with/without the extra tangential stress term, i.e., $(t_3 - t_1)\tilde{\tau}_{xx}$ in equation (2.4e). The presence of stable eigenvalues in the last column implicates extra tangential stress term in introducing the predicted instabilities.

yield stress leads to an extra tangential stress term, viz., $(t_3 - t_1)\tilde{\tau}_{xx}$ which not only destabilises GL modes but also gives rise to new unstable centre modes. Note that for $B = 0$, $t_1 = t_3$ and the destabilising term will vanish thereby indicating the role of fluid yield stress.

4.2. Hadamard instability

The dispersion curves shown in figure 5a showed instability even at high wavenumber, i.e., Hadamard instability. In this section, we demonstrate that the Hadamard instability can be removed by adding stress diffusivity term in the Saramito (2007) constitutive equation (2.2c). Note that, the stress diffusion term has been previously utilised by Fielding (2005) to ascribe finite length to the shear bands in plane shear flow of Johnson & Segalman (1977) fluid. Additionally, Buza *et al.* (2022); Beneitez *et al.* (2023); Couchman *et al.* (2024) predicted the existence of a new polymer diffusive instability in a PCF of a viscoelastic fluid nonzero solvent contribution. Here, we do not consider solvent contribution.

Upon addition of the stress diffusion term, the dimensionless constitutive equation becomes

$$W \left[\frac{\partial \boldsymbol{\tau}}{\partial t} + (\mathbf{v} \cdot \nabla) \boldsymbol{\tau} - (\nabla \mathbf{v})^T \cdot \boldsymbol{\tau} - \boldsymbol{\tau} \cdot (\nabla \mathbf{v}) \right] + \left[\frac{|\boldsymbol{\tau}_d| - B}{|\boldsymbol{\tau}_d|} \right] \boldsymbol{\tau} = \dot{\boldsymbol{\gamma}} + \epsilon \nabla^2 \boldsymbol{\tau}, \quad (4.1)$$

where $\epsilon = D^* G^* / (\eta^* R^{*2})$ is the scaled stress diffusivity with D^* as the dimensional stress diffusivity. The continuity and momentum equations given in (2.4) remain applicable. The linearised constitutive equation stress components are

$$\begin{aligned} & W [ik(\bar{v}_x - c)\tilde{\tau}_{xx} + \bar{v}_y D\tilde{\tau}_{xx} - 2ik\bar{\tau}_{xx}\bar{v}_x - 2D\bar{v}_x\tilde{\tau}_{xy} - 2\bar{\tau}_{xy}D\bar{v}_x] \\ & + \mathcal{F}[1 + (t_4 - t_2)\bar{\tau}_{xx}]\tilde{\tau}_{xx} + \mathcal{F}(t_3 - t_1)\bar{\tau}_{xx}\tilde{\tau}_{xy} - \mathcal{F}(t_4 - t_2)\bar{\tau}_{xx}\tilde{\tau}_{yy} \\ & = 2ik\bar{v}_x + \epsilon(D^2 - k^2)\tilde{\tau}_{xx}, \end{aligned} \quad (4.2)$$

$$\begin{aligned} & W [ik(\bar{v}_x - c)\tilde{\tau}_{xy} + \bar{v}_y D\tilde{\tau}_{xy} - ik\bar{\tau}_{xy}\bar{v}_x - D\bar{v}_x\tilde{\tau}_{yy} - ik\bar{\tau}_{xx}\bar{v}_y - \bar{\tau}_{xy}D\bar{v}_y] \\ & + \mathcal{F}[1 + (t_3 - t_1)\bar{\tau}_{xy}]\tilde{\tau}_{xy} + \mathcal{F}\bar{\tau}_{xy}(t_4 - t_2)(\tilde{\tau}_{xx} - \tilde{\tau}_{yy}) \\ & = (ik\bar{v}_y + D\bar{v}_x) + \epsilon(D^2 - k^2)\tilde{\tau}_{xy}, \end{aligned} \quad (4.3)$$

$$W [ik(\bar{v}_x - c)\tilde{\tau}_{yy} - 2ik\bar{\tau}_{xy}\bar{v}_y] + \mathcal{F}\tilde{\tau}_{yy} = 2D\bar{v}_y + \epsilon(D^2 - k^2)\tilde{\tau}_{yy}, \quad (4.4)$$

where the parameters \mathcal{F} , t_1 , t_2 , t_3 and t_4 remain unchanged. In addition to the boundary conditions specified in (2.5), six more boundary conditions will be necessary due to the stress diffusion term. Following Fielding (2005); Buza *et al.* (2022); Beneitez *et al.* (2023); Couchman *et al.* (2024), we consider vanishing stress derivatives at $y = 0, 1$,

$$D\tilde{\tau}_{xx} = 0; \quad D\tilde{\tau}_{xy} = 0; \quad D\tilde{\tau}_{yy} = 0. \quad (4.5)$$

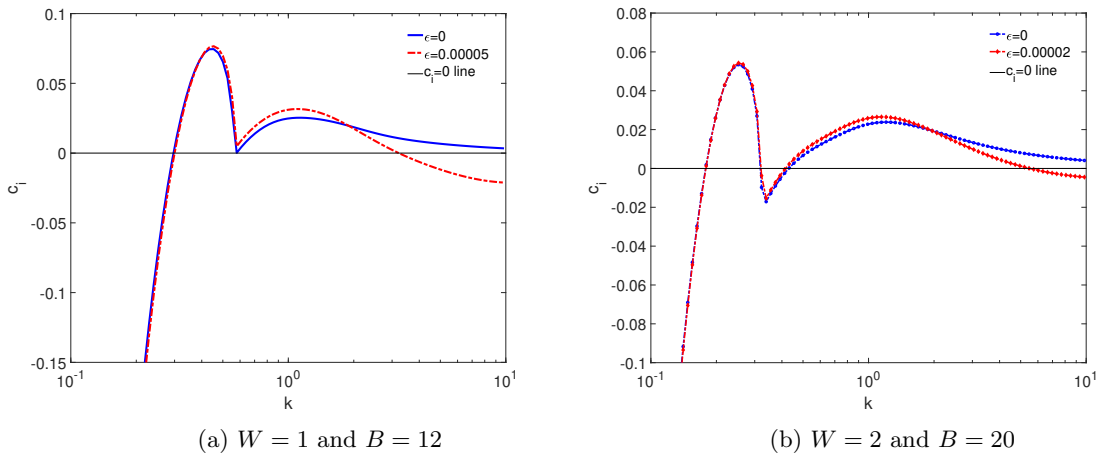


Figure 6: The effect of stress diffusivity on the dispersion curves. Panels show the stabilisation of the Hadamard instability as the stress diffusivity value increases for two sets of parameters.

The effect of nonzero stress diffusivity on the dispersion curves is shown in figure 6. For $\epsilon = 0$, the dispersion curve shows $c_i > 0$ even for $k = 10$. Although not shown here, this holds true for arbitrarily high wavenumber, signifying the presence of weak Hadamard instability. As ϵ assumes nonzero value even of $O(10^{-5})$, the perturbations at high wavenumber exhibit $c_i < 0$, implying stabilisation of arbitrarily high wavenumber instability. Thus, the stress diffusivity succeeds in removing weak Hadamard instability.

5. Conclusions

The linear stability of an elastoviscoplastic (EVP) plane Couette flow (PCF) is analysed using Saramito (2007) model. The pseudo-spectral method based on Chebyshev polynomials is employed to solve the eigenvalue problem. In the absence of yield stress, Saramito (2007) model reduces to the Upper Convected Maxwell (UCM) model.

The PCF of UCM exhibits two stable GL modes in the creeping-flow limit. As the yield stress effect, i.e., Bingham number, is increased, the GL modes become unstable. Additionally, a new class of modes travelling at the average speed of the fluid are destabilised, termed here as *centre modes*. Thus, analysis reveals two types of instabilities, viz., unstable GL modes and new centre modes. The analysis reveals that an extra tangential stress term arising due to the yield stress effect leads to the predicted instability. The dispersion curves are found to exhibit *weak Hadamard instability*, i.e., unstable perturbations of arbitrarily high wavenumber. The analysis demonstrates that an addition of stress diffusion term in the Saramito (2007) model can remove the Hadamard instability.

Declaration of interest

The author reports no conflict of interest.

Acknowledgments

The author acknowledges financial support from the SERB-DST under grant SRG/2023/000223.

REFERENCES

- ABDELGAWAD, M. S., CANNON, I. & ROSTI, M. E. 2023 Scaling and intermittency in turbulent flows of elastoviscoplastic fluids. *Nat. Phys.* pp. 1–5.
- APOSTOLIDIS, A. J. & BERIS, A. N. 2014 Modeling of the blood rheology in steady-state shear flows. *J. Rheol.* **58**(3), 607–633.
- ARORA, K., GANESAN, V., SURESHKUMAR, R. & KHOMAMI, B. 2004 Hydrodynamic stability of unidirectional shear flow of linear and branched polymeric melts. *J. Non-Newtonian Fluid Mech.* **121**, 101–115.
- BALMFORTH, N. J., FRIGAARD, I. A. & OVARLEZ, G. 2014 Yielding to stress: Recent developments in viscoplastic fluid mechanics. *Annu. Rev. Fluid Mech.* **46**, 121–146.
- BARRY, B. W. & MEYER, M. C. 1979 Rheological properties of carbopol gels. i: Continuous shear and creep properties of carbopol gels. *Int. J. Pharm.* **2**, 1–25.
- BENEITEZ, M., PAGE, J. & KERSWELL, R. R. 2023 Polymer diffusive instability leading to elastic turbulence in plane couette flow. *Phys. Rev. Fluids* **8** (10), L101901.
- BINGHAM, E. C. 1922 Fluidity and Plasticity. *McGraw-Hill Chap.* **VIII**, 215–218.
- BODIGUEL, H., BEAUMONT, H., MACHADO, A., MARTINIE, L., KELLAY, H. & COLIN, A. 2015 Flow enhancement due to elastic turbulence in channel flows of shear thinning fluids. *Phys. Rev. Lett.* **114**, 028302(5).
- BUZA, G., BENEITEZ, M., PAGE, J. & KERSWELL, R. R. 2022 Finite-amplitude elastic waves in viscoelastic channel flow from large to zero reynolds number. *Journal of Fluid Mechanics* **951**, A3.
- CASTILLO, H.A. & WILSON, H.J. 2017 Towards a mechanism for instability in channel flow of highly shear-thinning viscoelastic fluids. *J. Non-Newtonian Fluid Mech.* **247**, 15–21.
- CHANDRA, B., MANGAL, R., SHANKAR, V. & DAS, D. 2019 An instability driven by the shear-thinning and elasticity in the fluid flow of polymer solutions through microtubes. *Phys. Rev. Fluids* **4**, 083301.
- CHANDRA, B., SHANKAR, V. & DAS, D. 2018 Onset of transition in the flow of polymer solutions through microtubes. *J. Fluid Mech.* **844**, 1052–1083.
- CHAUDHARY, I., GARG, P., SHANKAR, V. & SUBRAMANIAN, G. 2019 Elasto-inertial wall mode instabilities in viscoelastic plane Poiseuille flow. *J. Fluid Mech.* **881**, 119–163.
- CHAUDHARY, I., GARG, P., SHANKAR, V. & SUBRAMANIAN, G. 2021 Linear instability of viscoelastic pipe flow. *J. Fluid Mech.* **908**, A11.
- CHOKSHI, P. & KUMARAN, V. 2009 Stability of the plane shear flow of dilute polymeric solutions. *Phys. Fluids* **21**, 014109.
- CHOUERI, G. H., LOPEZ, J. M. & HOF, B. 2018 Exceeding the asymptotic limit of polymer drag reduction. *Phys. Rev. Lett.* **120**, 124501.
- COUCHMAN, M. M. P., BUZA, G., BENEITEZ, M., PAGE, J. & KERSWELL, R. R. 2024 Inertial enhancement of the polymer diffusive instability. *J. Fluid Mech.* **981**, A2.
- CROMER, M., FREDRICKSON, G. H. & LEAL, L. G. 2014 A study of shear banding in polymer solutions. *Phys. Fluids* **26**, 063101.
- CROMER, M., VILLET, M. C., FREDRICKSON, G. H. & LEAL, L. G. 2013 Shear banding in polymer solutions. *Phys. Fluids* **26**, 051703.
- DATTA, S. S. ET AL. 2022 Perspectives on viscoelastic flow instabilities and elastic turbulence. *Physical Review Fluids* **7** (8), 080701.
- DONG, M. & ZHANG, M. 2022 Asymptotic study of linear instability in a viscoelastic pipe flow. *Journal of Fluid Mechanics* **935**, A28.
- ERKEN, O., FAZLA, B., MURADOGLU, M., IZBASSAROV, D., ROMANÒ, F. & GROTEBERG, J. B. 2023 Effects of elastoviscoplastic properties of mucus on airway closure in healthy and pathological conditions. *Phys. Rev. Fluids* **8**, 053102.
- FIELDING, SUZANNE M 2005 Linear instability of planar shear banded flow. *Phys. Rev. Lett.* **95** (13), 134501.

- FRAGGEDAKIS, D., DIMAKOPOULOS, Y. & TSAMOPOULOS, J. 2016 Yielding the yield stress analysis: A thorough comparison of recently proposed elasto-visco-plastic (evp) fluid models. *J. Non-Newt. Fluid Mech.* **236**, 104–122.
- FRIGAARD, I. A., HOWISON, S. D. & SOBEY, I. J. 1994 On the stability of poiseuille flow of a Bingham fluid. *J. Fluid Mech.* **263**, 133–150.
- GARG, P., CHAUDHARY, I., KHALID, M., SHANKAR, V. & SUBRAMANIAN, G. 2018 Viscoelastic pipe flow is linearly unstable. *Phys. Rev. Lett.* **121**, 024502.
- GIESEKUS, H. 1982 A simple constitutive equation for polymer fluids based on the concept of deformation-dependent tensorial mobility. *J. Non-Newtonian Fluid Mech.* **11**, 69–109.
- GORODTSOV, V. A. & LEONOV, A. I. 1967 On a linear instability of plane parallel Couette flow of viscoelastic fluid. *J. Appl. Math. Mech.* **31**, 289–299.
- GRILLET, A. M., BOGAERDS, A. C. B., PETERS, G. W. M. & BAAIJENS, F. P. T. 2002 Stability analysis of constitutive equations for polymer melts in viscometric flows. *J. Non-Newtonian Fluid Mech.* **103**, 221–250.
- HODA, N., JOVANOVIĆ, M. R. & KUMAR, S. 2008 Energy amplification in channel flows of viscoelastic fluids. *J. Fluid Mech.* **601**, 407–424.
- HODA, N., JOVANOVIĆ, M. R. & KUMAR, S. 2009 Frequency responses of streamwise-constant perturbations in channel flows of Oldroyd-B fluids. *J. Fluid Mech.* **625**, 411–434.
- IZBASSAROV, D., ROSTI, M. E., BRANDT, L. & TAMMISOLA, O. 2021 Effect of finite weissenberg number on turbulent channel flows of an elastoviscoplastic fluid. *J. Fluid Mech.* **927**, A45.
- JOHNSON, M. & SEGALMAN, D. 1977 A model for viscoelastic fluid behavior which allows non-affine deformation. *J. Non-Newtonian Fluid Mech.* **2**, 255–270.
- JOSEPH, D. D. & SAUT, J. C. 1986 Change of type and loss of evolution in the flow of viscoelastic fluids. *J. Non-Newtonian Fluid Mech.* **20**, 117–141.
- KHALID, M., SHANKAR, V. & SUBRAMANIAN, G. 2021 Continuous pathway between the elasto-inertial and elastic turbulent states in viscoelastic channel flow. *Physical Review Letters* **127**, 134502.
- LANDRY, M. P., FRIGAARD, I. A. & MARTINEZ, D. M. 2005 Stability and instability of Taylor–Couette flows of a Bingham fluid. *J. Fluid Mech.* **560**, 321–353.
- MOROZOV, A. N. & VAN SAARLOOS, W. 2005 Subcritical finite-amplitude solutions for plane Couette flow of viscoelastic fluids. *Phys. Rev. Lett.* **95**, 024501.
- MOYERS-GONZALEZ, M., BURGHELEA, T. I. & MAK, J. 2011 Linear stability analysis for plane-poiseuille flow of an elastoviscoplastic fluid with internal microstructure for large Reynolds numbers. *J. Non-Newton Fluid Mech* **166**, 515–531.
- NOUAR, C., BOTTARO, A. & BRANCHER, J. P. 2007a Delaying transition to turbulence in channel flow: Revisiting the stability of shear-thinning fluids. *J. Fluid Mech.* **592**, 177–194.
- NOUAR, C., KABOUYA, N., DUSEK, J. & MAMOU, M. 2007b Modal and non-modal linear stability of the plane bingham-poiseuille flow. *J. Fluid Mech.* **211**, 2843.
- PATNE, R., MANDLOI, S., SHANKAR, V. & SUBRAMANIAN, G. 2024 Instabilities in strongly shear-thinning viscoelastic flows through channels and tubes. *arXiv* p. 2408.01004.
- PATNE, R. & SHANKAR, V. 2018 Stability of flow through deformable channels and tubes: implications of consistent formulation. *J. Fluid Mech.* **860**, 837–885.
- PENG, J. & ZHU, K.-Q. 2004 Linear stability of Bingham fluids in spiral Couette flow. *J. Fluid Mech.* **512**, 21–45.
- PICAUT, L., RONSIN, O., CAROLI, C. & BAUMBERGER, T. 2017 Experimental evidence of a helical, supercritical instability in pipe flow of shear thinning fluids. *Phys. Rev. Fluids* **2**, 083303.
- POOLE, R. J. 2016 Elastic instabilities in parallel shear flows of a viscoelastic shear-thinning liquid. *Phys. Rev. Fluids* **1**, 041301.
- PUTZ, A. M. V. & BURGHELEA, T. I. 2009 The solid-fluid transition in a yield stress shear thinning physical gel. *Rheol. Acta* **48**, 673–689.
- RENARDY, M. & RENARDY, Y. 1986 Linear stability of plane Couette flow of an upper convected Maxwell fluid. *J. Non-Newtonian Fluid Mech.* **22**, 23–33.
- ROSTI, M. E., IZBASSAROV, D., TAMMISOLA, O., HORMOZI, S. & BRANDT, L. 2018 Turbulent channel flow of an elastoviscoplastic fluid. *J. Fluid Mech.* **853**, 488–514.

- SAHU, K. C., VALLURI, P., SPELT, P. D. M. & MATAR, O. K. 2007 Linear instability of pressure-driven channel flow of a newtonian and a herschel-bulkley fluid. *Phys. Fluids* **19**, 122101.
- SAMANTA, D., DUBIEF, Y., HOLZNER, M., SCHÄFER, C., MOROZOV, A. N., WAGNER, C. & HOF, B. 2013 Elasto-inertial turbulence. *Proc. Natl Acad. Sci. USA* **110**, 10557–10562.
- SARAMITO, P. 2007 A new constitutive equation for elastoviscoplastic fluid flows. *J Non-Newton Fluid Mech* **145**(1), 1–14.
- SCHMID, P. J. & HENNINGSON, D. S. 2001 *Stability and transition in shear flows*. New York: Springer.
- SHEMILT, J. D., HORSLEY, A., JENSEN, O. E., THOMPSON, A. B. & WHITFIELD, C. A. 2022 Surface-tension-driven evolution of a viscoplastic liquid coating the interior of a cylindrical tube. *J. Fluid Mech.* **944**, A22.
- SHEMILT, J. D., HORSLEY, A., JENSEN, O. E., THOMPSON, A. B. & WHITFIELD, C. A. 2023 Surfactant amplifies yield-stress effects in the capillary instability of a film coating a tube. *J. Fluid Mech.* **971**, A24.
- THIEN, N. P. & TANNER, R. I. 1977 A new constitutive equation derived from network theory. *J. Non-Newtonian Fluid Mech.* **2**, 353–365.
- TREFETHEN, L. N. 2000 *Spectral Methods in MATLAB*. Philadelphia: SIAM.
- WEN, C., POOLE, R. J., WILLIS, A. P. & DENNIS, D. J. C. 2017 Experimental evidence of symmetry-breaking supercritical transition in pipe flow of shear-thinning fluids. *Phys. Rev. Fluids* **2**, 031901.
- WHITE, J. L. & METZNER, A. B. 1963 Development of constitutive equations for polymeric melts and solutions. *J. Appl. Polym. Sci.* **7**, 1867–1889.
- WILSON, H.J. & LORIDAN, V. 2015 Linear instability of a highly shear-thinning fluid in channel flow. *J. Non-Newtonian Fluid Mech.* **223**, 200–208.
- WILSON, H.J. & RALLISON, J.M. 1999 Instability of channel flow of a shear-thinning White-Metzner fluid. *J. Non-Newtonian Fluid Mech.* **87**, 75–96.
- WILSON, H. J., RENARDY, M. & Y., RENARDY 1999 Structure of the spectrum in zero reynolds number shear flow of the ucm and oldroyd-b liquids. *J. Non-Newtonian Fluid Mech.* **80**, 251–268.